AGU ADVANCING EARTH AND SPACE SCIENCES

Geophysical Research Letters

RESEARCH LETTER
10.1029/2023GL106583

High *P-T* Sound Velocities of Amphiboles: Implications for Low-Velocity Anomalies in Metasomatized Upper Mantle

Wen-Yi Zhou[1], Ming Hao[2], Dongzhou Zhang[3,4], Przemyslaw Dera[3,4], Soisiri Charin[5], and Jin S. Zhang[1]

[1]Department of Geology and Geophysics, Texas A&M University, College Station, TX, USA, [2]Earth and Planets Laboratory, Carnegie Institution for Science, Washington, DC, USA, [3]Hawaii Institute of Geophysics and Planetology, University of Hawai'i at Mānoa, Honolulu, HI, USA, [4]Argonne National Laboratory, GeoSoiEnviroCARS, University of Chicago, Argonne, IL, USA, [5]Department of Earth and Environmental Sciences, University of Minnesota–Twin Cities, Minneapolis, MN, USA

Key Points:

- The single-crystal elasticity of tremolite is determined by Brillouin spectroscopy up to 7.3 GPa and 700 K
- Sound velocities of uppermost mantle amphiboles mainly depend on Fe content
- Hydrous minerals (amphiboles, serpentine, phlogopite) are plausible causes of the low velocity anomalies in the uppermost mantle

Supporting Information:

Supporting Information may be found in the online version of this article.

Correspondence to:

W.-Y. Zhou and J. S. Zhang,
wenyizhou.edu@hotmail.com;
jinzhang@tamu.edu

Citation:

Zhou, W.-Y., Hao, M., Zhang, D., Dera, P., Charin, S., & Zhang, J. S. (2024). High *P-T* sound velocities of amphiboles: Implications for low-velocity anomalies in metasomatized upper mantle. *Geophysical Research Letters*, *51*, e2023GL106583. https://doi.org/10.1029/2023GL106583

Received 27 SEP 2023
Accepted 16 FEB 2024

Abstract Metasomatized mantle xenoliths containing hydrous minerals, such as amphiboles, serpentine, and phlogopite, likely represent the potential mineralogical compositions of the metasomatized upper mantle, where low seismic velocities are commonly observed. This study presents the first experimentally determined single-crystal elasticity model of an Fe-free near Ca, Mg-endmember amphibole tremolite at high pressure and/or temperature conditions (maximum pressure 7.3(1) GPa, maximum temperature 700 K) using Brillouin spectroscopy. We found that sound velocities of amphiboles strongly depend on the Fe content. We then calculated the sound velocities of 441 hydrous-mineral-bearing mantle xenoliths collected around the globe, and quantitatively evaluated the roles that amphiboles, phlogopite and serpentine played in producing the low velocity anomalies in the metasomatized upper mantle.

Plain Language Summary Amphiboles are the most widely distributed hydrous minerals resulting from metasomatism in the upper most mantle. We measured sound velocities of tremolite (Ca, Mg endmember of the amphibole series) at high pressures and high temperatures by Brillouin spectroscopy. Based on global hydrous-mineral-bearing mantle xenoliths record, we quantitively evaluated the contributions of amphiboles, serpentine, and phlogopite to low velocity anomalies and water storage in the upper most mantle. We found the existence of hydrous minerals (amphiboles, serpentine, and phlogopite) remains a viable explanation for the low velocity anomalies in the upper most mantle (e.g., mid-lithosphere discontinuity). Compared to serpentine and phlogopite, although the amount of velocity reduction caused by amphibolization is moderate, the formation of amphiboles does not require K, Al, Si-rich environments like phlogopite, or exceedingly water-rich environments like serpentine.

1. Introduction

Water is usually transported to the deep Earth in the form of hydroxyl in mineral structures, thus quantifying the abundance and spatial distribution of hydrous minerals inside the Earth is crucial to understanding the water cycle and budget in the Earth's system (Ohtani, 2015). The most common hydrous minerals in the upper mantle xenoliths are amphiboles, serpentine, and phlogopite (PetDB database, https://doi.org/10.1594/IEDA/111309). Amphiboles can host ~2 wt% water and be stable up to 3 GPa at ~1000°C (Kovács et al., 2021). The pressure stability field of phlogopite, which contains ~3 wt% water, increases from 4 to 5 GPa at ~1300°C to 9 GPa at ~1000°C (Frost, 2006). Similarly, serpentine with ~13 wt% water, stable up to 7 GPa at 550°C, dehydrates at only 2.5 GPa when temperature exceeds 700°C (Kawamoto et al., 2013). Hydrous minerals are usually seismically slower than nominally anhydrous minerals (NAMs), the metamorphic reactions that form hydrous minerals from NAMs likely cause various low-velocity anomalies (e.g., Selway et al., 2015).

Under stable cratons, 2%–7% shear wave velocity (*Vs*) drops have been widely observed at 70–100 km depth (Fu et al., 2022; Rader et al., 2015). They are commonly interpreted as the mid-lithosphere discontinuity (MLD), since continental lithosphere is typically thicker than 130 km (Table S1 in Supporting Information S1). The formation mechanisms of MLD include: (a) partial melting (Thybo & Perchuć, 1997), (b) elastically accommodated grain-boundary sliding (Karato et al., 2015), (c) seismic anisotropy (e.g., Yuan & Romanowicz, 2010), (d) change in Mg# (Yuan & Romanowicz, 2010), and (e) hydrous minerals resulted from mantle metasomatism (Selway et al., 2015). Although Selway et al. (2015) suggested the existence of hydrous minerals among the most likely causes of MLD, this conclusion has been challenged by Saha et al. (2021). With ≤10 vol% amphibole and ≤2 vol% phlogopite in the globally averaged cratonic lithospheric mantle composition, the metasomatism induced *V*s reduction is only 2%–3% (Saha et al., 2021). Nevertheless, local chemical composition in metasomatized mantle can easily deviate from the global average, thus higher proportions and different combinations of hydrous minerals are possible (Tharimena et al., 2016; Wang & Kusky, 2019; Wölbern et al., 2012). Therefore, presence of hydrous minerals, such as amphiboles, serpentine, and phlogopite, is still a potential candidate to explain the MLD.

In subduction zones, low velocity layers have also been reported. Beneath NE Japan, a dipping low velocity layer (−10% *V*s) is observed atop the subducting Pacific slab, extending from ∼40 to ∼80 km depths (Kawakatsu & Watada, 2007; Nakajima et al., 2009; Tsuji et al., 2008). Interestingly, it gradually disappears at ∼80 km, and a new low velocity layer (−8% ∼ −10% *V*s) immediately appears and extends down to ∼130 km. This is possibly caused by the dehydration of lawsonite and amphiboles at ∼80 km depth and the subsequent formation of a serpentine and chlorite layer above the slab at ∼80–130 km (Kawakatsu & Watada, 2007; Tsuji et al., 2008). Understanding the distribution and abundance of different hydrous minerals in these low velocity layers can provide insights to water transport in subduction zones.

A few previous studies estimated the amount of hydrous minerals that are required to cause the aforementioned *V*s reductions in the upper mantle (Peng & Mookherjee, 2020; Rader et al., 2015). However, most of these studies utilized a simplified approach by increasing the fractions of hydrous minerals in a model peridotite (e.g., pyrolite) without considering actual reactions between different minerals. Saha et al. (2021) went one step further by considering previous phase equilibrium experiments, but covered limited composition space of the metasomatized upper mantle. The metasomatized upper mantle has strong compositional heterogeneity mainly due to wide compositional range of the migrating mantle melts/fluids (Batanova et al., 2011). Xenoliths records represent a much wider sampling of the mineralogical compositions in the metasomatized upper mantle (James et al., 2004; Kolesnichenko et al., 2017; Schutt & Lesher, 2010). The sound velocities of worldwide hydrous-mineral-bearing xenolith records are thus useful for quantitatively evaluating the contributions of different hydrous minerals to various upper mantle low velocity anomalies (James et al., 2004; Tommasi & Ishikawa, 2014).

Compared with serpentine and phlogopite, amphiboles are more abundant in mantle xenoliths (PetDB database). However, the *P-T* dependent single-crystal elastic properties of amphiboles are not well-constrained. Despite the two first-principles computational studies on tremolite and pargasite (Peng & Mookherjee, 2020; Saha et al., 2021), single-crystal elasticity of amphiboles has only been experimentally determined at ambient conditions (Brown & Abramson, 2016). Upper mantle amphiboles are complicated solid solutions usually between pargasite, edenite, tremolite, and actinolite. Separating the effects of different compositions on the elasticity of amphiboles is crucial. As the most important elemental substitution in mantle minerals, Fe-Mg substitution has a first-order effect on the elasticity of amphiboles. Due to the complex Na, Al-Si coupled substitution in pargasite, studying Fe-Mg solid solution is more straightforward in tremolite. Thus, we conducted the first single-crystal Brillouin spectroscopy experiments on Fe-free tremolite at pressures up to 7.3 (1) GPa and temperatures up to 700 K. In conjunction with previous studies on serpentine, phlogopite, and Fe-bearing amphiboles, we estimated the effect of Fe on the sound velocities of amphiboles, calculated sound velocities of 441 hydrous-mineral-bearing xenoliths worldwide, and finally modeled the effects of different hydrous minerals on low velocity anomalies in the upper mantle.

2. Methods

2.1. Experiments

We double-side polished three natural tremolite crystals from Merelani, Tanzania, to ∼20 μm thick, inspected them to be inclusion and scratch free under microscope, then measured the chemical composition using the JEOL 8200 Electron Microprobe Analyzer (EPMA) hosted at the University of New Mexico (UNM). The unit cell parameters at ambient condition and the planes normal of the crystals were determined using the single-crystal X-ray diffractometer at the X-ray Atlas Diffraction Lab at the University of Hawaiʻi at Mānoa and sector 13-BM-C, GeosoilEnviorCars (GSECARS), Advanced Photon Source (APS), Argonne National Laboratory (ANL) (Text S1 in Supporting Information S1). Using the obtained unit cell parameters a = 9.915(1) Å, b = 17.983 (1) Å, c = 5.296(1) Å, β = 105.352(5)° and the chemical composition $(Na_{0.040(5)}K_{0.020(4)})Ca_{2.00(1)}(Mg_{4.90(3)}Mn_{0.009(2)})(Si_{7.82(2)}Al_{0.28(1)})O_{22}(OH_{1.90(1)},F_{0.10(1)})$ (Tables S2 and S3 in Supporting Information S1), ambient density (ρ_0)

10.1029/2023GL106583

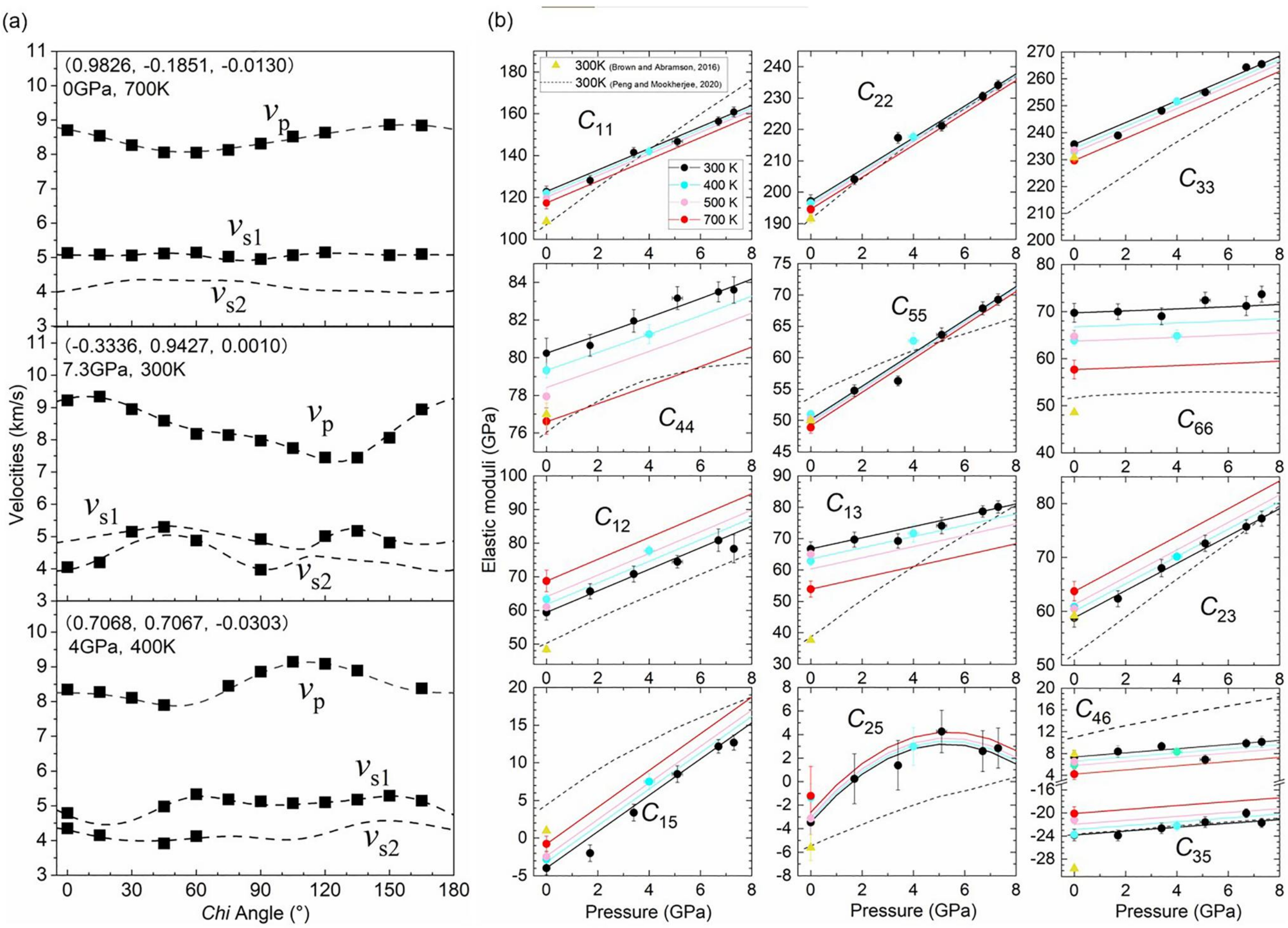

Figure 1. (a) Comparison between experimentally measured sound velocity data (squares) and the sound velocities predicted from the best-fit C_{ij} model for different crystals at different *P-T* conditions. The error bars of individual sound velocity measurements are smaller than the symbols. (b) C_{ij}s of tremolite in this study (some error bars are smaller than symbols) and previous studies. Solid lines represent finite strain EOS fitting results in this study. C_{ij}s by local density approximation in Peng and Mookherjee (2020) have been transformed to match the Cartesian coordinate system used in this study and Brown and Abramson (2016).

was calculated as 2.97 (2) g/cm^3. The planes of the three crystals are (0.7068, 0.7067, −0.0303), (0.9826, −0.1851, −0.0130), and (−0.3336, 0.9427, 0.0010) in fractional coordinates.

Three polished crystals were then loaded into three different BX90 Diamond Anvil Cells (DACs) with 450 μm culet diamonds. The sample chamber was created by drilling a 280 μm-diameter hole in a preindented ∼55 μm thick Re gasket. Two ruby spheres were loaded as pressure markers (Datchi et al., 2007). Argon or neon was loaded as pressure-transmitting medium (Rivers et al., 2008). High temperatures were generated by a platinum resistive heater and measured by two K-type thermocouples glued near the diamond culet (Lai et al., 2020). Temperature differences given by two thermocouples were less than 15 K up to 700 K.

Brillouin spectroscopy experiments were conducted under 50° symmetric forward scattering geometry using a 532 nm single-mode laser. The scattering angle calibrated using Corning 7980 glass was 50.4°. Compressional wave velocities (*V*p) and *V*s were measured at 36 Chi angles at each *P-T* condition (Figure 1a). Figure S2 in Supporting Information S1 shows typical Brillouin spectra. We conducted experiments at 0 GPa up to 700 K, and at 300 K up to 7.3(1) GPa. Simultaneously high *P-T* data were only acquired at 4.0 (2) GPa 400 K with dozens of trials (Text S2 in Supporting Information S1).

2.2. Modeling

We analyzed 4473 mantle xenoliths data with published mineral proportions from the PetDB database and found that amphiboles, serpentine and phlogopite are the most prevalent hydrous minerals, present in ∼6.8%, ∼3.0%, and ~2.7% of all xenoliths, respectively. Other hydrous minerals are less common (e.g., chlorite: ~0.3%, lawsonite: <0.1%). Additionally, we incorporated xenolith data from publications not included in PetDB (see Data Availability Statement). A total of 441 mantle xenoliths data were selected and used in this study using four criteria: (a) containing amphiboles, phlogopite or serpentine; (b) excluding samples that were altered on the Earth's surface; (c) no melt (glass); (d) containing <1 vol% of carbonate minerals, opaque minerals (e.g., magnetite) and other less common hydrous minerals.

We calculated *V*p and *V*s of metasomatized upper mantle lithologies represented by xenoliths with amphiboles/phlogopite/serpentine at 2.5 GPa and 973 K under Voigt-Reuss-Hill averaging scheme, using thermoelastic properties of minerals summarized in Tables S5 and S6 of the Supporting Information S1 and the 3rd or 4th order finite strain equation of state (EOS) (Texts S3 and S4 in Supporting Information S1).

3. Results and Discussion

3.1. Elastic Properties of Tremolite

We utilized the conventional settings defined by the Institute of Electrical and Electronics engineers to align the cartesian coordinates for elasticity tensor with respect to the monoclinic fractional coordinates (Brainerd et al., 1949): Y//b-axis, Z//c-axis, X//a*, which is perpendicular to Y and Z. With the measured *V*p-*V*s data set along different phonon directions of tremolite, we used Christoffel equation to calculate the best-fit C_{ij} model at each *P*-*T* condition (Figure 1). Most C_{ij}s are well-constrained as evidenced by the sensitivity test and trade-off correlation matrices (Figure S3, Table S8 in Supporting Information S1). The non-ambient condition densities, *P*-*T* derivatives of *K*s, *G* and C_{ij}s are calculated based on the *P*-*T*-*V*p-*V*s data set using temperature-dependent 3rd/4th order finite strain EOS (Davies & Dziewonski, 1975; Duffy & Anderson, 1989). The details are shown in Text S4 of the Supporting Information S1.

All 13 single-crystal elastic moduli (C_{ij}s) of tremolite increase with pressure (Figure 1). The diagonal C_{ij}s, C_{13}, and C_{46} decrease with temperature, while C_{12}, C_{23}, C_{15}, C_{25}, and C_{35} unexpectedly increase with temperature. As a chain silicate, tremolite's elastic stiffness is heavily controlled by the topology of the Si tetrahedra network. T1 silicate tetrahedra of tremolite shows negative thermal expansion at room-pressure high-temperature conditions (Sueno et al., 1973), causing tetrahedral chain shrinkage along [010] direction and stronger distortion between T1 and T2 tetrahedra at high temperatures (Hawthorne & Grundy, 1976). A shrinked tetrahedra chain with increased distortion is likely more resistant to stress, resulting in positive temperature derivatives of C_{12} and C_{23}. Future studies are needed to quantitatively validate this hypothesis.

At ambient condition, most C_{ij}s (e.g., C_{11}, C_{22}, C_{33}) of the tremolite sample in this study are larger than those of the Fe-bearing tremolite in Brown and Abramson (2016) (Figure 1b). Although the absolute values of some ambient condition C_{ij}s of end-member tremolite ($Ca_2Mg_5(Si_8O_{22})(OH)_2$) computationally determined by Peng and Mookherjee (2020) are very different from this study (e.g., C_{33}, C_{55}, C_{13}, C_{23}), they actually converge with the values presented in this study at high-pressure conditions. Most of the C_{ij}s which do not converge at higher pressures share similar pressure derivatives (e.g., C_{22}, C_{12}, C_{44}, C_{66}) between this study and Peng and Mookherjee (2020). We also calculated the linear compressibilities of tremolite based on the ambient C_{ij}s: β_a (0.005 GPa^{-1}) > β_b (0.0027 GPa^{-1}) > β_c (0.0021 GPa^{-1}) (Table S9 in Supporting Information S1). This general relationship is consistent with what was found in previous XRD experiments (Comodi et al., 1991; Ott et al., 2023), although β_a and β_c obtained in this study are smaller than the values given in Ott et al. (2023). Peng and Mookherjee (2020) and Brown and Abramson (2016) both suggested β_a (0.0063 GPa^{-1}) > β_c (0.0027 GPa^{-1}) > β_b (0.0026 GPa^{-1}). The inconsistencies between these studies are likely related to different chemical compositions (e.g., F, Al, and Fe) and the use of different methods (e.g., computation vs. experiment).

In terms of aggregate elastic properties, within the *P*-*T* range we studied, no abrupt sound velocity changes were observed as a result of the compression mechanism change at ~5 GPa suggested by Ott et al. (2023). The best-fit aggregate elastic properties are: Ks_0 = 98 (5) GPa, G_0 = 62 (3) GPa, $(\partial Ks/\partial P)_{T0}$ = 3.5 (1), $(\partial G/\partial P)_{T0}$ = 1.15 (5), $(\partial Ks/\partial T)_{P0}$ = −0.004 (2) GPa/K, and $(\partial G/\partial T)_{P0}$ = −0.011 (1) GPa/K. Compared with multiple Fe-bearing amphibole samples measured in Brown and Abramson (2016), the Fe-free near endmember tremolite measured in this study shows the highest sound velocities (Figure 2b). As shown in Figures 2b–2d, *V*p and *V*s of amphiboles decrease almost linearly with Fe content, whereas their correlations with Al content or A site occupation seem weak. Compared with previous static compression XRD studies, the Ks_0 of 98 (5) GPa and $(\partial Ks/\partial P)_{T0}$ of 3.5 (1)

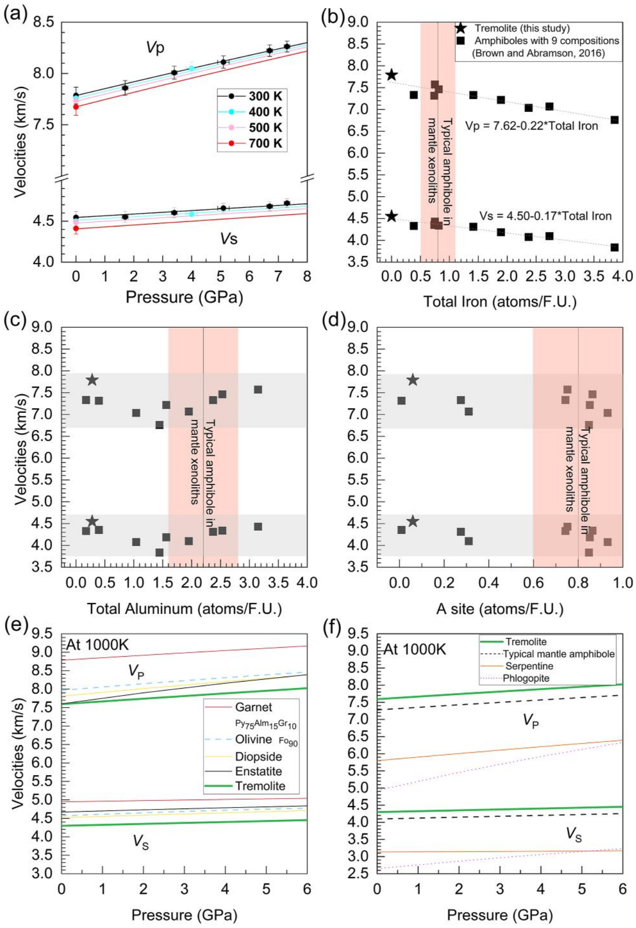

Figure 2. (a) V_P and V_S of isotropic polycrystalline tremolite aggregates as a function of pressure along different isotherms in this study. Solid lines represent 3rd order finite strain EOS fitting results for tremolite in this study. Effect of (b) Fe, (c) Al, and (d) A site occupation on sound velocities of amphiboles at ambient condition. (e) Sound velocities of tremolite and upper mantle NAMs. (f) Sound velocities of tremolite, typical mantle amphibole, serpentine and phlogopite. The elasticity data used to calculate sound velocities of minerals are compiled in Table S6 of the Supporting Information S1. The shaded red region in (b) shows the Fe content range of typical amphiboles from mantle xenoliths, the shaded gray regions in (d) and (c) show that Al content and A site occupation have limited effects on sound velocities of amphiboles. *V*p and *V*s are reduced by 220 and 170 m/s if the total Fe atom number per formula unit (F.U.) increases by 1.

obtained in this study are significantly higher and lower than the K_{T0} of 72 (7) GPa and $(\partial K_{T0}/\partial P)_{T0}$ of 8.6 (42) obtained in Ott et al. (2023), which cannot be explained by the difference between isothermal and adiabatic elasticity. Instead, it is related to the higher F content in the tremolite sample used in Ott et al. (2023), which can soften the bulk and shear modulus of amphiboles (e.g., glaucophane, Mookherjee & Bezacier, 2012), as well as the well-known tradeoffs between K_{T0} and $(\partial K_{T0}/\partial P)_{T0}$ in static compression XRD studies.

The average chemical composition of mantle amphiboles was calculated from the 142 EPMA composition records from the mantle xenoliths database (El Messbahi et al., 2015; Ho et al., 2006; Kaczmarek et al., 2016a; Matusiak-Małek et al., 2017a; Tilhac et al., 2016). An average chemical composition is obtained as $Na_{0.9(3)}K_{0.2(1)}Ca_{1.7(1)}Mg_{3.6(4)}Fe_{0.8(3)}Al_{2.2(6)}Si_{6.3(4)}O_{22}(OH)_2$, which is similar to sample 8 measured in Brown and Abramson (2016). Utilizing the ambient elasticity data of sample 8 in Brown and Abramson (2016), and the *P-T* derivatives of the elastic moduli determined in this study, we calculated the sound velocities of a typical mantle amphibole (Figure 2f). As expected, both tremolite and the typical mantle amphibole are seismically slower than NAMs, but faster than phlogopite and antigorite (Figures 2e and 2f).

Tremolite has high elastic anisotropy, the single-crystal *V*p and *V*s azimuthal anisotropy as well as *V*s radial anisotropy are ~30% at 0–3 GPa. Kim and Jung (2019) suggested that deformed amphibolites can produce 2%–13% *V*p and *V*s azimuthal anisotropy depending on the type of crystal preferred orientation (CPO). Unfortunately, CPO data of amphiboles are limited in xenolith records, distinguishing the primary CPOs formed in the mantle from the secondary CPOs formed during exhumation remains challenging (Puziewicz et al., 2023). Therefore, elastic anisotropy of tremolite was not considered in our modeling. Future studies are needed to take this important factor into account.

3.2. Hydrous Minerals in Xenoliths

Most hydrous-mineral-bearing xenoliths are peridotite or pyroxenite, with some amphibolite or serpentinite. Amphiboles tend to coexist with clinopyroxene in xenoliths (Figure S1a in Supporting Information S1). Previous petrological studies have noted that amphibole and clinopyroxene grains tend to be juxtaposed in the lherzolite xenoliths from Alaska and North China Craton (Francis, 1976; Wang et al., 2021; Xu et al., 2010). This mineral association is explained by: (a) amphiboles and clinopyroxenes found in xenoliths are both enriched in Ca and Mg; (b) clinopyroxenes and amphiboles are both near-liquidus phases of interstitial melts in the hydrous basalt-peridotite reaction experiments (Wang et al., 2021). In contrast, serpentine fraction is negatively correlated with olivine and orthopyroxene fractions (Figure S1c in Supporting Information S1), since serpentine grows at the expense of olivine and orthopyroxene during mantle metasomatism (Andréani et al., 2007). A recent study suggested that amphiboles are not stable in a typical hydrated upper mantle with 50–200 ppm water along a continental geotherm (Juriček & Keppler, 2023). However, with increasing water activity, the stability field of amphiboles is displaced to higher pressures and lower temperatures. As shown in Figure 4e, amphibole-bearing metasomatized lithospheric mantle can host up to 2 wt% water, the existence of amphiboles in cold cratonic mantle, at least locally, cannot be excluded.

3.3. Sound Velocities of Hydrous-Mineral-Bearing Xenoliths

We explored the relationship between *V*p, *V*s and different mineral proportions in mantle xenoliths (Figure 3). For the xenoliths with <5 vol% serpentine/phlogopite, olivine abundance has little effect on sound velocities because

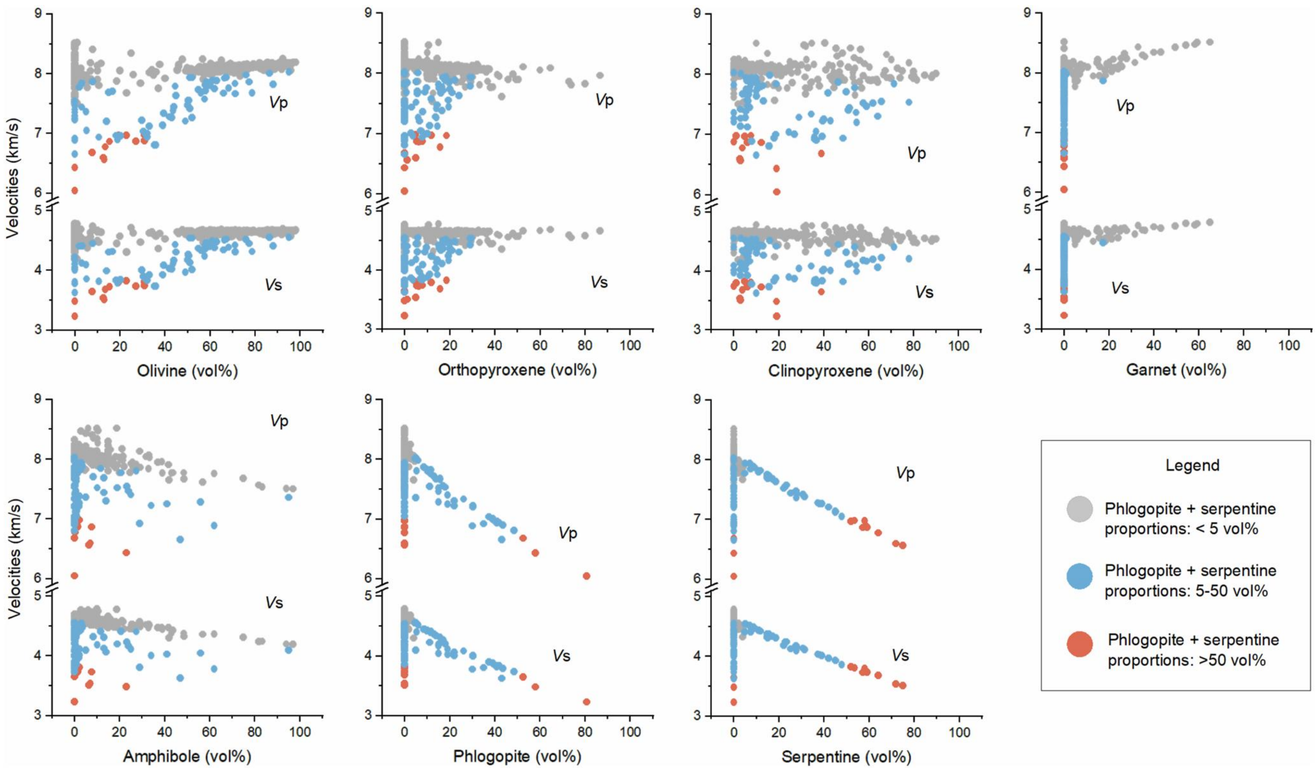

Figure 3. Effects of (a) olivine, (b) orthopyroxene, (c) clinopyroxene, (d) garnet, (e) amphiboles, (f) phlogopite, (g) serpentine proportions on the sound velocities of hydrous-mineral-bearing xenoliths.

olivine shares similar sound velocities with other NAMs when compared to hydrous minerals. For the xenoliths with >5 vol% serpentine/phlogopite, their sound velocities increase with olivine fractions since phlogopite/serpentine grows at the expense of olivine. The relationships between pyroxene fractions and sound velocities of xenoliths are similar (Figures 3b and 3c), and can be explained similarly.

Garnet mainly exists in the xenoliths with <5 vol% serpentine/phlogopite (Figure 3d). Increasing garnet abundance leads to higher sound velocities since garnet is seismically faster than other upper mantle NAMs (Figure 2e). Conversely, high amphiboles, phlogopite, or serpentine fractions decrease sound velocities. The effects of phlogopite and serpentine are stronger than amphiboles since they are seismically slower (Figure 2f).

4. Implications

Amphiboles are found to coexist with either serpentine or phlogopite in mantle xenoliths, but not both (Table S4 in Supporting Information S1). The effects of amphibole and serpentine, as well as amphibole and phlogopite abundance, on the sound velocities of metasomatized upper mantle lithologies are shown in Figures 4a–4d. Assuming amphiboles, phlogopite, and serpentine contain ∼2, 3, and 13 wt% water, respectively, we calculated the seismic velocity reduction caused by different hydration levels in the upper mantle (Figures 4e and 4f).

4.1. Implications for the Velocity Drop at MLD

To achieve the observed 2%–7% *V*s reduction at MLD under continental cratons (Fu et al., 2022; Rader et al., 2015) (Table S1 in Supporting Information S1), 10–60 vol% amphiboles, 3–15 vol% phlogopite, or 5–15 vol% serpentine are required (Figures 4a–4d). 3–15 vol% phlogopite or serpentine are commonly found in xenoliths (Figures S1e and S1f in Supporting Information S1). Although amphibolites with ∼60 vol% amphiboles are rare (Figure S1d in Supporting Information S1), the wide coexistence between amphiboles and serpentine/phlogopite in xenoliths records can easily explain the 2%–7% *V*s reduction at MLD (Figure 4, e.g. Wilcza Gora, Matusiak-Małek et al., 2017a). Thus, existence of hydrous minerals cannot be ruled out as a potential explanation

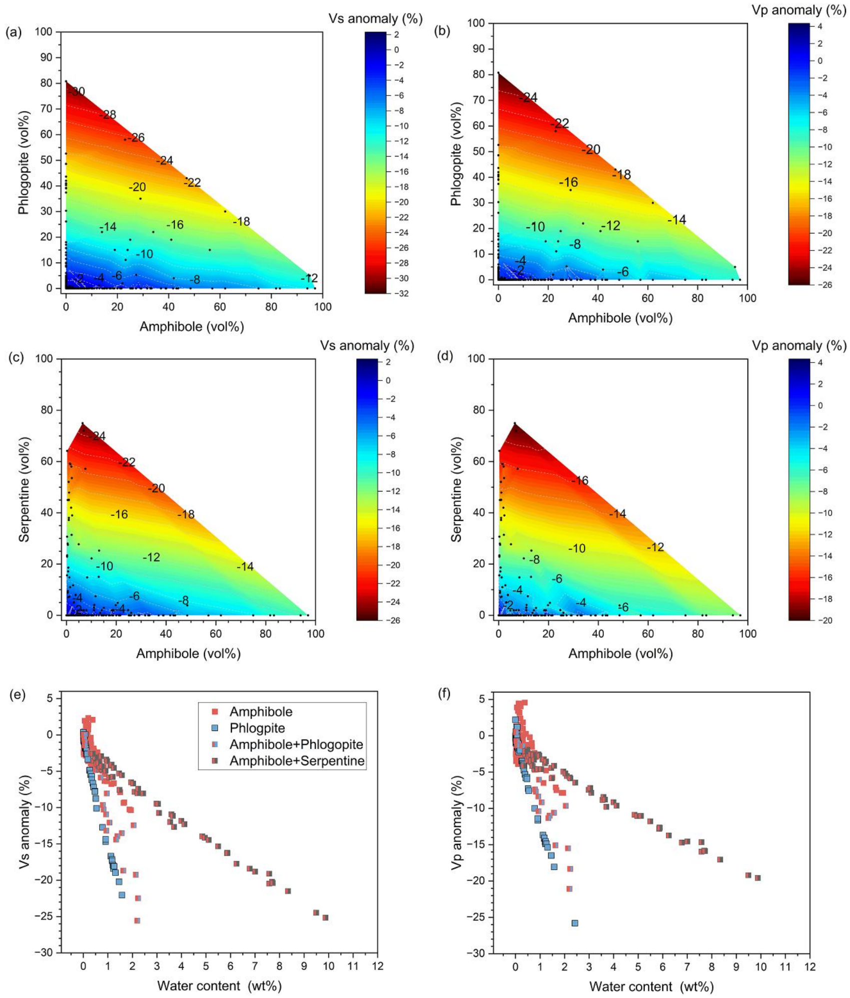

Figure 4. (a) *V*s, and (b) *V*p anomalies of metasomatized mantle rocks resulted from (co)existence of amphibole or phlogopite. (c) *V*s, and (d) *V*p anomalies of metasomatized mantle rocks resulted from (co)existence of amphibole or serpentine. (e) *V*s, and (f) *V*p anomalies of metasomatized mantle rocks as a function of bulk rock water content. In (a)–(d), the dots refer to *V*p and *V*s anomalies calculated from xenolith data in Table S4 of the Supporting Information S1, and the numbers refer to *V*p and *V*s anomalies along different contours.

for MLD, at least locally. According to Figure 4e, 2%–7% *V*s reduction suggests ~0.3–2 wt% water is likely stored at MLD depths if metasomatism is the main cause.

Significant *V*s drops of 12%–24% have also been reported under East Africa at 50–100 km depths, with a 12% *V*s reduction beneath the Tanzania Craton and a 24% *V*s reduction below the Albert-Edward rift (Wölbern et al., 2012). Due to the very high abundance of the phlogopite-rich xenoliths found in these regions, Wölbern et al. (2012) proposed that the MLD under East Africa was related to an altered lithospheric mantle enriched in phlogopite, resulted from melt infiltration. A 12% *V*s reduction could be explained by a metasomatized mantle containing ~30 vol% phlogopite (Figure 4a), consistent with the record from local xenoliths (Wölbern et al., 2012). However, a 24% *V*s reduction beneath the Albert-Edward rift would require >60 vol% phlogopite, which is rarely observed in nature. Therefore, an alternative explanation is needed (e.g., partial melt, Thybo and Perchuć (1997)).

4.2. Implications for the Low Velocity Layers Atop Subducting Slabs

Kawakatsu and Watada (2007) and Tsuji et al. (2008) have identified a dipping low velocity layer (−8% to −10% *V*s) above the Pacific slab at 80–130 km depths under NE Japan. This layer is interpreted as a hydrous mineral-rich layer, mainly composed of serpentine, formed by the reactions between slab-derived fluids and peridotites (Tsuji et al., 2008). If this is true, according to Figure 4, the −8% to −10% low velocity anomalies above the Pacific slab could be explained by 20–25 vol% serpentine, corresponding to ∼2%–3% water in the mantle wedge beneath NE Japan.

4.3. Velocity Reduction Efficiency With Limited Water Supply in the Mantle

To achieve the same velocity reduction, the serpentinized mantle requires 3–4 times more water than the phlogopite-bearing mantle, with the amphibole-bearing but phlogopite/serpentine-free mantle in between (Figures 4e and 4f). Although the sound velocities of amphiboles are only moderately low compared with mantle NAMs, the amount of water that is needed to form amphiboles is small (only ∼2 wt%) compared with serpentine (∼13 wt%). Therefore, with the same amount of water supply, amphibolization is more effective in reducing the seismic velocities than serpentinization. Similarly, despite the moderately low water content (∼3 wt%) in phlogopite, its sound velocities are even lower than serpentine, making it the most efficient seismic velocity reducer in the metasomatized upper mantle. The formation of phlogopite, serpentine, and amphiboles in nature is controlled by many factors: parent rock composition, melt composition, *P-T* conditions, etc (Nielson et al., 1993a). For example, K, Al, Si-rich fluids derived from the top sedimentary layer of subducting slabs could react with peridotite to form phlogopite, while serpentine is a common metasomatism product in ultramafic/mafic lithologies (Bryant et al., 2007; Poli & Schmidt, 2002). Compared to serpentine and phlogopite, amphiboles' formation is less restricted by parent rock or fluid composition, due to their highly flexible crystal structures with 7 different cation sites (Hawthorne et al., 2007). Consequently, amphiboles can form in different hydrous uppermost mantle settings, as seen in the wide coexistence of amphiboles with either serpentine or phlogopite in xenolith records (Figures 4a–4d, Table S4 in Supporting Information S1). As shown in Figures 4a–4d, there is no clear relationship between the amphiboles fraction and phlogopite/serpentine fraction. Future investigations of the relationship between different mineral proportions with respect to the whole rock composition and water content are needed for better quantification of the seismic velocity reduction caused by metasomatism in the Earth's upper mantle.

Data Availability Statement

The first part of mantle xenolith data used in this study is publicly available in PetDB Database (https://doi.org/10.1594/IEDA/111309). The second part of mantle xenolith data used in this research that is not included in PetDB is available in Gorring and Kay (2000a), Ho et al. (2000a), Ionov et al. (2002a), Kaczmarek et al. (2016a), Matusiak-Małek et al. (2017a), Nielson et al. (1993a), Powell et al. (2004a), Raffone et al. (2009a), Rosatelli et al. (2007a), Smith et al. (1999a), Szabó and Taylor (1994a), and Xu et al. (2003a). All derived mantle xenolith data from PetDB and previous publications are available via Zenodo through the following link: https://doi.org/10.5281/zenodo.7909294.

Acknowledgments
We thank Mike Spilde for his help in EPMA at UNM, Young Jay Ryu for DAC gas loading, Ye Peng, Andreas Kronenberg, and Willian Lamb for useful discussions. Use of APS was supported by the US Department of Energy under Contract No.DE-AC02-06CH11357. This project is funded by NSF-EAR 2243184 (JSZ).

References

Andréani, M., Mével, C., Boullier, A. M., & Escartin, J. (2007). Dynamic control on serpentine crystallization in veins: Constraints on hydration processes in oceanic peridotites. *Geochemistry, Geophysics, Geosystems*, *8*, Q02012. https://doi.org/10.1029/2006gc001373

Batanova, V., Belousov, I., Savelieva, G., & Sobolev, A. (2011). Consequences of channelized and diffuse melt transport in supra-subduction zone mantle: Evidence from the Voykar Ophiolite (Polar Urals). *Journal of Petrology*, *52*(12), 2483–2521. https://doi.org/10.1093/petrology/egr053

Brainerd, J., Jensen, A., Cumming, L., Batcher, R., Begun, S., Black, H., et al. (1949). Standards on piezoelectric crystals. *Proceedings of the IRE*, *37*(12), 1378–1395.

Brown, J. M., & Abramson, E. H. (2016). Elasticity of calcium and calcium-sodium amphiboles. *Physics of the Earth and Planetary Interiors*, *261*, 161–171. https://doi.org/10.1016/j.pepi.2016.10.010

Bryant, J., Yogodzinski, G., & Churikova, T. (2007). Melt-mantle interactions beneath the Kamchatka arc: Evidence from ultramafic xenoliths from Shiveluch volcano. *Geochemistry, Geophysics, Geosystems*, *8*, Q04007. https://doi.org/10.1029/2006gc001443

Comodi, P., Mellini, M., Ungaretti, L., & Zanazzi, P. F. (1991). Compressibility and high pressure structure refinement of tremolite, pargasite and glaucophane. *European Journal of Mineralogy*, *3*(3), 485–499. https://doi.org/10.1127/ejm/3/3/0485

Datchi, F., Dewaele, A., Loubeyre, P., Letoullec, R., Le Godec, Y., & Canny, B. (2007). Optical pressure sensors for high-pressure–high-temperature studies in a diamond anvil cell. *High Pressure Research*, *27*(4), 447–463. https://doi.org/10.1080/08957950701659593

Davies, G., & Dziewonski, A. (1975). Homogeneity and constitution of the Earth's lower mantle and outer core. *Physics of the Earth and Planetary Interiors*, *10*(4), 336–343. https://doi.org/10.1016/0031-9201(75)90060-6

Duffy, T. S., & Anderson, D. L. (1989). Seismic velocities in mantle minerals and the mineralogy of the upper mantle. *Journal of Geophysical Research*, *94*(B2), 1895–1912. https://doi.org/10.1029/jb094ib02p01895

El Messbahi, H., Bodinier, J.-L., Vauchez, A., Dautria, J.-M., Ouali, H., & Garrido, C. J. (2015). Short wavelength lateral variability of lithospheric mantle beneath the Middle Atlas (Morocco) as recorded by mantle xenoliths. *Tectonophysics*, *650*, 34–52. https://doi.org/10.1016/j.tecto.2014.11.020

Francis, D. (1976). The origin of amphibole in lherzolite xenoliths from Nunivak Island, Alaska. *Journal of Petrology*, *17*(3), 357–378. https://doi.org/10.1093/petrology/17.3.357

Frost, D. J. (2006). The stability of hydrous mantle phases. *Reviews in Mineralogy and Geochemistry*, *62*(1), 243–271. https://doi.org/10.2138/rmg.2006.62.11

Fu, H. Y., Li, Z. H., & Chen, L. (2022). Continental mid-lithosphere discontinuity: A water collector during craton evolution. *Geophysical Research Letters*, *49*(23), e2022GL101569. https://doi.org/10.1029/2022gl101569

Gorring, M. L., & Kay, S. M. (2000a). Carbonatite metasomatized peridotite xenoliths from southern Patagonia: Implications for lithospheric processes and Neogene Plateau magmatism [Dataset]. Contributions to Mineralogy and Petrology, *140*(1), 55–72. https://doi.org/10.1007/s004100000164

Hawthorne, F., & Grundy, H. (1976). The crystal chemistry of the amphiboles; IV, X-ray and neutron refinements of the crystal structure of tremolite. *The Canadian Mineralogist*, *14*(3), 334–345.

Hawthorne, F. C., Oberti, R., Della Ventura, G., & Mottana, A. (2007). Amphiboles: Crystal chemistry: Amphiboles: Crystal chemistry, occurrence, and health issues. *Reviews in Mineralogy and Geochemistry*, *67*, 1–54. https://doi.org/10.2138/rmg.2007.67.1

Ho, K., Chen, J., & Chung, S. (2006). Composite mantle xenoliths in basaltic pyroclastic rocks from Tungchihsu, Penghu Islands, Taiwan Strait: Evidence for a metasomatized lithospheric mantle beneath SE China. *Collection and Research*, *19*, 49–76.

Ho, K.-S., Chen, J.-C., Smith, A. D., & Juang, W.-S. (2000a). Petrogenesis of two groups of pyroxenite from Tungchihsu, Penghu Islands, Taiwan Strait: Implications for mantle metasomatism beneath SE China [Dataset]. *167*(3–4), 355–372. https://doi.org/10.1016/s0009-2541(99)00237-5

Ionov, D. A., Bodinier, J.-L., Mukasa, S. B., & Zanetti, A. (2002a). Mechanisms and sources of mantle metasomatism: Major and trace element compositions of peridotite xenoliths from Spitsbergen in the context of numerical modelling [Dataset]. Journal of Petrology, *43*(12), 2219–2259. https://doi.org/10.1093/petrology/43.12.2219

James, D. E., Boyd, F., Schutt, D., Bell, D., & Carlson, R. (2004). Xenolith constraints on seismic velocities in the upper mantle beneath southern Africa. *Geochemistry, Geophysics, Geosystems*, *5*, Q01002. https://doi.org/10.1029/2003gc000551

Juriček, M. P., & Keppler, H. (2023). Amphibole stability, water storage in the mantle, and the nature of the lithosphere-asthenosphere boundary. *Earth and Planetary Science Letters*, *608*, 118082. https://doi.org/10.1016/j.epsl.2023.118082

Kaczmarek, M.-A., Bodinier, J.-L., Bosch, D., Tommasi, A., Dautria, J.-M., & Kechid, S. (2016a). Metasomatized mantle xenoliths as a record of the lithospheric mantle evolution of the northern edge of the Ahaggar Swell, in Teria (Algeria). *Journal of Petrology*, *57*(2), 345–382. https://doi.org/10.1093/petrology/egw009

Karato, S.-I., Olugboji, T., & Park, J. (2015). Mechanisms and geologic significance of the mid-lithosphere discontinuity in the continents. *Nature Geoscience*, *8*(7), 509–514. https://doi.org/10.1038/ngeo2462

Kawakatsu, H., & Watada, S. (2007). Seismic evidence for deep-water transportation in the mantle. *Science*, *316*(5830), 1468–1471. https://doi.org/10.1126/science.1140855

Kawamoto, T., Yoshikawa, M., Kumagai, Y., Mirabueno, M. H. T., Okuno, M., & Kobayashi, T. (2013). Mantle wedge infiltrated with saline fluids from dehydration and decarbonation of subducting slab. *Proceedings of the National Academy of Sciences of the United States of America*, *110*(24), 9663–9668. https://doi.org/10.1073/pnas.1302040110

Kim, J., & Jung, H. (2019). New crystal preferred orientation of amphibole experimentally found in simple shear. *Geophysical Research Letters*, *46*(22), 12996–13005. https://doi.org/10.1029/2019gl085189

Kolesnichenko, M. V., Zedgenizov, D. A., Litasov, K. D., Safonova, I. Y., & Ragozin, A. L. (2017). Heterogeneous distribution of water in the mantle beneath the central Siberian Craton: Implications from the Udachnaya Kimberlite Pipe. *Gondwana Research*, *47*, 249–266. https://doi.org/10.1016/j.gr.2016.09.011

Kovács, I. J., Liptai, N., Koptev, A., Cloetingh, S. A., Lange, T. P., Maţenco, L., et al. (2021). The 'pargasosphere' hypothesis: Looking at global plate tectonics from a new perspective. *Global and Planetary Change*, *204*, 103547. https://doi.org/10.1016/j.gloplacha.2021.103547

Lai, X., Zhu, F., Zhang, J. S., Zhang, D., Tkachev, S., Prakapenka, V. B., & Chen, B. (2020). An externally-heated diamond anvil cell for synthesis and single-crystal elasticity determination of Ice-VII at high pressure-temperature conditions. *Journal of Visualized Experiments*, (160), e61389. https://doi.org/10.3791/61389-v

Matusiak-Małek, M., Puziewicz, J., Ntaflos, T., Grégoire, M., Kukuła, A., & Wojtulek, P. M. (2017a). Origin and evolution of rare amphibole-bearing mantle peridotites from Wilcza Góra (SW Poland), Central Europe. *Lithos*, *286*, 302–323. https://doi.org/10.1016/j.lithos.2017.06.017

Mookherjee, M., & Bezacier, L. (2012). The low velocity layer in subduction zone: Structure and elasticity of glaucophane at high pressures. *Physics of the Earth and Planetary Interiors*, *208*, 50–58. https://doi.org/10.1016/j.pepi.2012.07.007

Nakajima, J., Tsuji, Y., Hasegawa, A., Kita, S., Okada, T., & Matsuzawa, T. (2009). Tomographic imaging of hydrated crust and mantle in the subducting Pacific slab beneath Hokkaido, Japan: Evidence for dehydration embrittlement as a cause of intraslab earthquakes. *Gondwana Research*, *16*(3–4), 470–481. https://doi.org/10.1016/j.gr.2008.12.010

Nielson, J., Budahn, J., Unruh, D., & Wilshire, H. (1993a). Actualistic models of mantle metasomatism documented in a composite xenolith from Dish Hill. *Geochimica et Cosmochimica Acta*, *57*(1), 105–121. https://doi.org/10.1016/0016-7037(93)90472-9

Ohtani, E. (2015). Hydrous minerals and the storage of water in the deep mantle. *Chemical Geology*, *418*, 6–15. https://doi.org/10.1016/j.chemgeo.2015.05.005

Ott, J. N., Kalkan, B., Kunz, M., Berlanga, G., Yuvali, A. F., & Williams, Q. (2023). Structural behavior of C2/m tremolite to 40 GPa: A high-pressure single-crystal X-ray diffraction study. *American Mineralogist*, *108*(5), 903–914. https://doi.org/10.2138/am-2022-8278

Peng, Y., & Mookherjee, M. (2020). Thermoelasticity of tremolite amphibole: Geophysical implications: American mineralogist. *Journal of Earth and Planetary Materials*, *105*(6), 904–916. https://doi.org/10.2138/am-2020-7189

Poli, S., & Schmidt, M. W. (2002). Petrology of subducted slabs. *Annual Review of Earth and Planetary Sciences*, *30*(1), 207–235. https://doi.org/10.1146/annurev.earth.30.091201.140550

Powell, W., Zhang, M., O'Reilly, S. Y., & Tiepolo, M. (2004a). Mantle amphibole trace-element and isotopic signatures trace multiple metasomatic episodes in lithospheric mantle, western Victoria, Australia [Dataset]. Lithos, *75*(1–2), 141–171. https://doi.org/10.1016/j.lithos.2003.12.017

Puziewicz, J., Aulbach, S., Kaczmarek, M. A., Ntaflos, T., Gerdes, A., Mazurek, H., et al. (2023). The origin and evolution of DMM-like lithospheric mantle beneath continents: Mantle xenoliths from the Oku Volcanic Group in the Cameroon Volcanic Line, West Africa. *Journal of Petrology*, *64*(7), egad049. https://doi.org/10.1093/petrology/egad049

Rader, E., Emry, E., Schmerr, N., Frost, D., Cheng, C., Menard, J., et al. (2015). Characterization and petrological constraints of the midlithospheric discontinuity. *Geochemistry, Geophysics, Geosystems*, *16*(10), 3484–3504. https://doi.org/10.1002/2015gc005943

Raffone, N., Chazot, G., Pin, C., Vannucci, R., & Zanetti, A. (2009a). Metasomatism in the lithospheric mantle beneath Middle Atlas (Morocco) and the origin of Fe-and Mg-rich wehrlites [Dataset]. Journal of Petrology, *50*(2), 197–249. https://doi.org/10.1093/petrology/egn069

Rivers, M., Prakapenka, V. B., Kubo, A., Pullins, C., Holl, C. M., & Jacobsen, S. D. (2008). The COMPRES/GSECARS gas-loading system for diamond anvil cells at the Advanced Photon Source. *High Pressure Research*, *28*(3), 273–292. https://doi.org/10.1080/08957950802333593

Rosatelli, G., Wall, F., & Stoppa, F. (2007a). Calcio-carbonatite melts and metasomatism in the mantle beneath Mt. Vulture (Southern Italy) [Dataset]. Lithos, *99*(3–4), 229–248. https://doi.org/10.1016/j.lithos.2007.05.011

Saha, S., Peng, Y., Dasgupta, R., Mookherjee, M., & Fischer, K. M. (2021). Assessing the presence of volatile-bearing mineral phases in the cratonic mantle as a possible cause of mid-lithospheric discontinuities. *Earth and Planetary Science Letters*, *553*, 116602. https://doi.org/10.1016/j.epsl.2020.116602

Schutt, D. L., & Lesher, C. E. (2010). Compositional trends among Kaapvaal Craton garnet peridotite xenoliths and their effects on seismic velocity and density. *Earth and Planetary Science Letters*, *300*(3–4), 367–373. https://doi.org/10.1016/j.epsl.2010.10.018

Selway, K., Ford, H., & Kelemen, P. (2015). The seismic mid-lithosphere discontinuity. *Earth and Planetary Science Letters*, *414*, 45–57. https://doi.org/10.1016/j.epsl.2014.12.029

Smith, D., Riter, J. A., & Mertzman, S. A. (1999a). Water–rock interactions, orthopyroxene growth, and Si-enrichment in the mantle: Evidence in xenoliths from the Colorado Plateau, southwestern United States [Dataset]. Earth and Planetary Science Letters, *165*(1), 45–54. https://doi.org/10.1016/s0012-821x(98)00251-9

Sueno, S., Cameron, M., Papike, J., & Prewitt, C. (1973). The high temperature crystal chemistry of tremolite: American mineralogist. *Journal of Earth and Planetary Materials*, *58*(7–8), 649–664.

Szabó, C., & Taylor, L. A. (1994a). Mantle petrology and geochemistry beneath the Nógrád-Gömör volcanic field, Carpathian-Pannonian region [Dataset]. International Geology Review, *36*(4), 328–358. https://doi.org/10.1080/00206819409465465

Tharimena, S., Rychert, C. A., & Harmon, N. (2016). Seismic imaging of a mid-lithospheric discontinuity beneath Ontong Java Plateau. *Earth and Planetary Science Letters*, *450*, 62–70. https://doi.org/10.1016/j.epsl.2016.06.026

Thybo, H., & Perchuć, E. (1997). The seismic 8 discontinuity and partial melting in continental mantle. *Science*, *275*(5306), 1626–1629. https://doi.org/10.1126/science.275.5306.1626

Tilhac, R., Ceuleneer, G., Griffin, W. L., O'Reilly, S. Y., Pearson, N. J., Benoit, M., et al. (2016). Primitive arc magmatism and delamination: Petrology and geochemistry of pyroxenites from the Cabo Ortegal Complex, Spain. *Journal of Petrology*, *57*(10), 1921–1954. https://doi.org/10.1093/petrology/egw064

Tommasi, A., & Ishikawa, A. (2014). Microstructures, composition, and seismic properties of the Ontong Java Plateau mantle root. *Geochemistry, Geophysics, Geosystems*, *15*(11), 4547–4569. https://doi.org/10.1002/2014gc005452

Tsuji, Y., Nakajima, J., & Hasegawa, A. (2008). Tomographic evidence for hydrated oceanic crust of the Pacific slab beneath northeastern Japan: Implications for water transportation in subduction zones. *Geophysical Research Letters*, *35*, L14308. https://doi.org/10.1029/2008gl034461

Wang, C., Liang, Y., & Xu, W. (2021). Formation of amphibole-bearing peridotite and amphibole-bearing pyroxenite through hydrous melt-peridotite reaction and in situ crystallization: An experimental study. *Journal of Geophysical Research: Solid Earth*, *126*(3), e2020JB019382. https://doi.org/10.1029/2020jb019382

Wang, Z., & Kusky, T. M. (2019). The importance of a weak mid-lithospheric layer on the evolution of the cratonic lithosphere. *Earth-Science Reviews*, *190*, 557–569. https://doi.org/10.1016/j.earscirev.2019.02.010

Wölbern, I., Rümpker, G., Link, K., & Sodoudi, F. (2012). Melt infiltration of the lower lithosphere beneath the Tanzania craton and the Albertine rift inferred from S receiver functions. *Geochemistry, Geophysics, Geosystems*, *13*, Q0AK08. https://doi.org/10.1029/2012gc004167

Xu, W., Yang, D., Gao, S., Pei, F., & Yu, Y. (2010). Geochemistry of peridotite xenoliths in Early Cretaceous high-Mg# diorites from the Central Orogenic Block of the North China Craton: The nature of Mesozoic lithospheric mantle and constraints on lithospheric thinning. *Chemical Geology*, *270*(1–4), 257–273. https://doi.org/10.1016/j.chemgeo.2009.12.006

Xu, X., O'Reilly, S. Y., Griffin, W., & Zhou, X. (2003a). Enrichment of upper mantle peridotite: Petrological, trace element and isotopic evidence in xenoliths from SE China [Dataset]. Chemical Geology, *198*(3–4), 163–188. https://doi.org/10.1016/s0009-2541(03)00004-4

Yuan, H., & Romanowicz, B. (2010). Lithospheric layering in the North American craton. *Nature*, *466*(7310), 1063–1068. https://doi.org/10.1038/nature09332

References From the Supporting Information

Kaczmarek, M.-A., Bodinier, J.-L., Bosch, D., Tommasi, A., Dautria, J.-M., & Kechid, S. (2016b). Metasomatized mantle xenoliths as a record of the lithospheric mantle evolution of the northern edge of the Ahaggar Swell, in Teria (Algeria) [Dataset]. Journal of Petrology, *57*(2), 345–382. https://doi.org/10.1093/petrology/egw009

Matusiak-Małek, M., Puziewicz, J., Ntaflos, T., Grégoire, M., Kukuła, A., & Wojtulek, P. M. (2017b). Origin and evolution of rare amphibole-bearing mantle peridotites from Wilcza Góra (SW Poland), Central Europe [Dataset]. Lithos, *286*, 302–323. https://doi.org/10.1016/j.lithos.2017.06.017

Nielson, J., Budahn, J., Unruh, D., & Wilshire, H. (1993b). Actualistic models of mantle metasomatism documented in a composite xenolith from Dish Hill [Dataset]. Geochimica et Cosmochimica Acta, *57*(1), 105–121. https://doi.org/10.1016/0016-7037(93)90472-9

Alemayehu, M., Zhang, H.-F., & Aulbach, S. (2017). Persistence of fertile and hydrous lithospheric mantle beneath the northwestern Ethiopian Plateau: Evidence from modal, trace element and Sr–Nd–Hf isotopic compositions of amphibole-bearing mantle xenoliths. *Lithos*, *284*, 401–415. https://doi.org/10.1016/j.lithos.2017.04.021

Arimoto, T., Gréaux, S., Irifune, T., Zhou, C., & Higo, Y. (2015). Sound velocities of $Fe_3Al_2Si_3O_{12}$ almandine up to 19 GPa and 1700 K. *Physics of the Earth and Planetary Interiors*, *246*, 1–8. https://doi.org/10.1016/j.pepi.2015.06.004

Armytage, R. M., Brandon, A. D., Peslier, A. H., & Lapen, T. J. (2014). Osmium isotope evidence for Early to Middle Proterozoic mantle lithosphere stabilization and concomitant production of juvenile crust in Dish Hill, CA peridotite xenoliths. *Geochimica et Cosmochimica Acta*, *137*, 113–133. https://doi.org/10.1016/j.gca.2014.04.017

Baptiste, V., Tommasi, A., & Demouchy, S. (2012). Deformation and hydration of the lithospheric mantle beneath the Kaapvaal craton, South Africa. *Lithos*, *149*, 31–50. https://doi.org/10.1016/j.lithos.2012.05.001

Bass, J. D., & Weidner, D. J. (1984). Elasticity of single-crystal orthoferrosilite. *Journal of Geophysical Research*, *89*(B6), 4359–4371. https://doi.org/10.1029/jb089ib06p04359

Bodin, T., Yuan, H., & Romanowicz, B. (2014). Inversion of receiver functions without deconvolution—Application to the Indian craton. *Geophysical Journal International*, *196*(2), 1025–1033. https://doi.org/10.1093/gji/ggt431

Bonatti, E., Ottonello, G., & Hamlyn, P. R. (1986). Peridotites from the island of Zabargad (St. John), Red Sea: Petrology and geochemistry. *Journal of Geophysical Research*, *91*(B1), 599–631. https://doi.org/10.1029/jb091ib01p00599
Brown, J., Slutsky, L., Nelson, K., & Cheng, L. T. (1989). Single-crystal elastic constants for San Carlos peridot: An application of impulsive stimulated scattering. *Journal of Geophysical Research*, *94*(B7), 9485–9492. https://doi.org/10.1029/jb094ib07p09485
Brueckner, H. K., Van Roermund, H. L., & Pearson, N. J. (2004). An Archean (?) to Paleozoic evolution for a garnet peridotite lens with sub-Baltic shield affinity within the Seve Nappe Complex of Jämtland, Sweden, Central Scandinavian Caledonides. *Journal of Petrology*, *45*(2), 415437.
Bruker, A. (2017). *Version 2017.3-0*. Bruker AXS: Inc.
Canil, D., O'Neill, H. S. C., Pearson, D., Rudnick, R. L., McDonough, W. F., & Carswell, D. (1994). Ferric iron in peridotites and mantle oxidation states. *Earth and Planetary Science Letters*, *123*(1–3), 205–220. https://doi.org/10.1016/0012-821x(94)90268-2
Chesley, J. T., Rudnick, R. L., & Lee, C.-T. (1999). Re-Os systematics of mantle xenoliths from the East African Rift: Age, structure, and history of the Tanzanian craton. *Geochimica et Cosmochimica Acta*, *63*(7–8), 1203–1217. https://doi.org/10.1016/s0016-7037(99)00004-6
Choi, S. H., Suzuki, K., Mukasa, S. B., Lee, J.-I., & Jung, H. (2010). Lu–Hf and Re–Os systematics of peridotite xenoliths from Spitsbergen, western Svalbard: Implications for mantle–crust coupling. *Earth and Planetary Science Letters*, *297*(1–2), 121–132. https://doi.org/10.1016/j.epsl.2010.06.013
Conceicao, R. V., Mallmann, G., Koester, E., Schilling, M., Bertotto, G., & Rodriguez-Vargas, A. (2005). Andean subduction-related mantle xenoliths: Isotopic evidence of Sr–Nd decoupling during metasomatism. *Lithos*, *82*(3–4), 273–287. https://doi.org/10.1016/j.lithos.2004.09.022
Darbyshire, F. A., Eaton, D. W., & Bastow, I. D. (2013). Seismic imaging of the lithosphere beneath Hudson Bay: Episodic growth of the Laurentian mantle keel. *Earth and Planetary Science Letters*, *373*, 179–193. https://doi.org/10.1016/j.epsl.2013.05.002
Davies, G. (1974). Effective elastic moduli under hydrostatic stress—I. Quasi-harmonic theory. *Journal of Physics and Chemistry of Solids*, *35*(11), 1513–1520. https://doi.org/10.1016/s0022-3697(74)80279-9
De Hoog, J. C., Gall, L., & Cornell, D. H. (2010). Trace-element geochemistry of mantle olivine and application to mantle petrogenesis and geothermobarometry. *Chemical Geology*, *270*(1–4), 196–215. https://doi.org/10.1016/j.chemgeo.2009.11.017
de Vries, J., Jacobs, M. H. G., van den Berg, A. P., Wehber, M., Lathe, C., McCammon, C. A., & van Westrenen, W. (2013). Thermal equation of state of synthetic orthoferrosilite at lunar pressures and temperatures. *Physics and Chemistry of Minerals*, *40*(9), 691–703. https://doi.org/10.1007/s00269-013-0605-5
Dera, P., Zhuravlev, K., Prakapenka, V., Rivers, M. L., Finkelstein, G. J., Grubor-Urosevic, O., et al. (2013). High pressure single-crystal micro X-ray diffraction analysis with GSE_ADA/RSV software. *High Pressure Research*, *33*(3), 466–484. https://doi.org/10.1080/08957959.2013.806504
Downes, H., Macdonald, R., Upton, B. G., Cox, K. G., Bodinier, J.-L., Mason, P. R., et al. (2004). Ultramafic xenoliths from the Bearpaw Mountains, Montana, USA: Evidence for multiple metasomatic events in the lithospheric mantle beneath the Wyoming craton. *Journal of Petrology*, *45*(8), 1631–1662. https://doi.org/10.1093/petrology/egh027
Ehrenberg, S. N. (1982). Petrogenesis of garnet lherzolite and megacrystalline nodules from the Thumb, Navajo volcanic field. *Journal of Petrology*, *23*(4), 507–547. https://doi.org/10.1093/petrology/23.4.507
Fei, Y. (1995). Thermal expansion: Mineral physics and crystallography: A handbook of physical constants. *2*, 29–44.
Finger, L. W., & Ohashi, Y. (1976). The thermal expansion of diopside to 800°C and a refinement of the crystal structure at 700° C. *American Mineralogist*, *61*(3–4), 303–310.
Frey, F. A., & Prinz, M. (1978). Ultramafic inclusions from San Carlos, Arizona: Petrologic and geochemical data bearing on their petrogenesis. *Earth and Planetary Science Letters*, *38*(1), 129–176. https://doi.org/10.1016/0012-821x(78)90130-9
Glaser, S. M., Foley, S. F., & Günther, D. (1999). Trace element compositions of minerals in garnet and spinel periodotite xenoliths from the Vitim volcanic field, Transbaikalia, eastern Siberia. *Developments in Geotectonics*, *24*, 263–285.
Goncharov, A., Nikitina, L., Borovkov, N., Babushkina, M., & Sirotkin, A. (2015). Thermal and redox equilibrium conditions of the upper-mantle xenoliths from the Quaternary volcanoes of NW Spitsbergen, Svalbard Archipelago. *Russian Geology and Geophysics*, *56*(11), 1578–1602. https://doi.org/10.1016/j.rgg.2015.10.006
González-Jiménez, J. M., Villaseca, C., Griffin, W. L., O'Reilly, S. Y., Belousova, E., Ancochea, E., & Pearson, N. J. (2014). Significance of ancient sulfide PGE and Re–Os signatures in the mantle beneath Calatrava, Central Spain. *Contributions to Mineralogy and Petrology*, *168*(2), 1–24. https://doi.org/10.1007/s00410-014-1047-x
Gorring, M. L., & Kay, S. M. (2000b). Carbonatite metasomatized peridotite xenoliths from southern Patagonia: Implications for lithospheric processes and Neogene Plateau magmatism. *Contributions to Mineralogy and Petrology*, *140*(1), 55–72. https://doi.org/10.1007/s004100000164
Griffin, W., Nikolic, N., O'Reilly, S. Y., & Pearson, N. (2012). Coupling, decoupling and metasomatism: Evolution of crust–mantle relationships beneath NW Spitsbergen. *Lithos*, *149*, 115–135. https://doi.org/10.1016/j.lithos.2012.03.003
Gu, X., Ingrin, J., Deloule, E., France, L., & Xia, Q. (2018). Metasomatism in the sub-continental lithospheric mantle beneath the South French Massif Central: Constraints from trace elements, Li and H in peridotite minerals. *Chemical Geology*, *478*, 2–17. https://doi.org/10.1016/j.chemgeo.2017.08.006
Gudelius, D., Aulbach, S., Braga, R., Höfer, H. E., Woodland, A. B., & Gerdes, A. (2019). Element transfer and redox conditions in continental subduction zones: New insights from peridotites of the Ulten Zone, North Italy. *Journal of Petrology*, *60*(2), 231–268. https://doi.org/10.1093/petrology/egy112
Halama, R., Savov, I. P., Rudnick, R. L., & McDonough, W. F. (2009). Insights into Li and Li isotope cycling and sub-arc metasomatism from veined mantle xenoliths, Kamchatka. *Contributions to Mineralogy and Petrology*, *158*(2), 197–222. https://doi.org/10.1007/s00410-009-0378-5
Hao, M., Zhang, J. S., Pierotti, C. E., Zhou, W.-Y., Zhang, D., & Dera, P. (2020). The seismically fastest chemical heterogeneity in the Earth's deep upper mantle—Implications from the single-crystal thermoelastic properties of jadeite. *Earth and Planetary Science Letters*, *543*, 116345. https://doi.org/10.1016/j.epsl.2020.116345
Hao, M., Zhang, J. S., Zhou, W. Y., & Wang, Q. (2021). Seismic visibility of eclogite in the Earth's upper mantle—Implications from high pressure-temperature single-crystal elastic properties of omphacite. *Journal of Geophysical Research: Solid Earth*, *126*(5), e2021JB021683. https://doi.org/10.1029/2021jb021683
Ho, K.-S., Chen, J.-C., Smith, A. D., & Juang, W.-S. (2000b). Petrogenesis of two groups of pyroxenite from Tungchihsu, Penghu Islands, Taiwan Strait: Implications for mantle metasomatism beneath SE China. *Chemical Geology*, *167*(3–4), 355–372. https://doi.org/10.1016/s0009-2541(99)00237-5
Hugh-Jones, D. (1997). Thermal expansion of $MgSiO_3$ and $FeSiO_3$ ortho-and clinopyroxenes. *American Mineralogist*, *82*(7–8), 689–696. https://doi.org/10.2138/am-1997-7-806

Ionov, D. A. (2007). Compositional variations and heterogeneity in fertile lithospheric mantle: Peridotite xenoliths in basalts from Tariat, Mongolia. *Contributions to Mineralogy and Petrology*, *154*(4), 455–477. https://doi.org/10.1007/s00410-007-0203-y

Ionov, D. A., Bodinier, J.-L., Mukasa, S. B., & Zanetti, A. (2002b). Mechanisms and sources of mantle metasomatism: Major and trace element compositions of peridotite xenoliths from Spitsbergen in the context of numerical modelling. *Journal of Petrology*, *43*(12), 2219–2259. https://doi.org/10.1093/petrology/43.12.2219

Ionov, D. A., Doucet, L. S., Xu, Y., Golovin, A. V., & Oleinikov, O. B. (2018). Reworking of Archean mantle in the NE Siberian craton by carbonatite and silicate melt metasomatism: Evidence from a carbonate-bearing, dunite-to-websterite xenolith suite from the Obnazhennaya kimberlite. *Geochimica et Cosmochimica Acta*, *224*, 132–153. https://doi.org/10.1016/j.gca.2017.12.028

Irifune, T., Higo, Y., Inoue, T., Kono, Y., Ohfuji, H., & Funakoshi, K. (2008). Sound velocities of majorite garnet and the composition of the mantle transition region. *Nature*, *451*(7180), 814–817. https://doi.org/10.1038/nature06551

Isse, T., Suetsugu, D., Ishikawa, A., Shiobara, H., Sugioka, H., Ito, A., et al. (2021). Seismic evidence for a thermochemical mantle plume underplating the lithosphere of the Ontong Java Plateau. *Communications Earth & Environment*, *2*(1), 98. https://doi.org/10.1038/s43247-021-00169-9

Jackson, J. M., Sinogeikin, S. V., & Bass, J. D. (2007). Sound velocities and single-crystal elasticity of orthoenstatite to 1073K at ambient pressure. *Physics of the Earth and Planetary Interiors*, *161*(1–2), 1–12. https://doi.org/10.1016/j.pepi.2006.11.002

Jeffcoate, A., Elliott, T., Kasemann, S., Ionov, D., Cooper, K., & Brooker, R. (2007). Li isotope fractionation in peridotites and mafic melts. *Geochimica et Cosmochimica Acta*, *71*(1), 202–218. https://doi.org/10.1016/j.gca.2006.06.1611

Juteau, T., Berger, E., & Cannat, M. (1990). Serpentinized, residual mantle peridotites from the MAR median valley, ODP Hole 670A (21 10′N, 45 02′W, Leg 109): Primary mineralogy and geothermometry. In *Proceedings of ocean drilling program. Scientific results* (Vol. 106, p. 109).

Kandelin, J., & Weidner, D. J. (1988). Elastic properties of hedenbergite. *Journal of Geophysical Research*, *93*(B2), 1063–1072. https://doi.org/10.1029/jb093ib02p01063

Kung, J., Li, B., Uchida, T., & Wang, Y. (2005). In-situ elasticity measurement for the unquenchable high-pressure clinopyroxene phase: Implication for the upper mantle. *Geophysical Research Letters*, *32*, L01307. https://doi.org/10.1029/2004gl021661

Lee, C., & Rudnick, R. (1999). Compositionally stratified cratonic lithosphere: Petrology and geochemistry of peridotite xenoliths from the Labait tuff cone, Tanzania. In *Proceedings of the 7th international Kimberlite conference* (pp. 503–521).

Li, B., & Neuville, D. R. (2010). Elasticity of diopside to 8GPa and 1073K and implications for the upper mantle. *Physics of the Earth and Planetary Interiors*, *183*(3–4), 398–403. https://doi.org/10.1016/j.pepi.2010.08.009

Li, H. Y., Chen, R. X., Zheng, Y. F., Hu, Z., & Xu, L. (2018). Crustal metasomatism at the slab-mantle interface in a continental subduction channel: Geochemical evidence from orogenic peridotite in the Sulu orogen. *Journal of Geophysical Research: Solid Earth*, *123*(3), 2174–2198. https://doi.org/10.1002/2017jb014015

Liu, J., Chen, G., Gwanmesia, G. D., & Liebermann, R. C. (2000). Elastic wave velocities of pyrope– majorite garnets ($Py_{62}Mj_{38}$ and $Py_{50}Mj_{50}$) to 9 GPa. *Physics of the Earth and Planetary Interiors*, *120*(1–2), 153–163. https://doi.org/10.1016/s0031-9201(00)00152-7

Magganas, A., & Koutsovitis, P. (2015). Composition, melting and evolution of the upper mantle beneath the Jurassic Pindos Ocean inferred by ophiolitic ultramafic rocks in East Othris, Greece. *International Journal of Earth Sciences*, *104*(5), 1185–1207. https://doi.org/10.1007/s00531-014-1137-z

Meng, F., Ai, Y., Xu, T., Chen, L., Wang, X., & Li, L. (2021). Lithospheric structure beneath the boundary region of North China Craton and Xing Meng Orogenic Belt from S-receiver function analysis. *Tectonophysics*, *818*, 229067. https://doi.org/10.1016/j.tecto.2021.229067

Njombie, M. P. W., Temdjim, R., & Foley, S. F. (2018). Petrology of spinel lherzolite xenoliths from Youkou volcano, Adamawa Massif, Cameroon Volcanic Line: Mineralogical and geochemical fingerprints of sub-rift mantle processes. *Contributions to Mineralogy and Petrology*, *173*(2), 1–20. https://doi.org/10.1007/s00410-018-1438-5

Pearson, N., Griffin, W., Doyle, B., O'Reilly, S., Van Achterbergh, E., & Kivi, K. (1998). Xenoliths from kimberlite pipes of the Lac de Gras area, Slave craton, Canada. *Proceedings of the International Kimberlite Conference: Extended abstracts* (Vol. 7, pp. 670–672).

Perinelli, C., Gaeta, M., & Armienti, P. (2017). Cumulate xenoliths from Mt. Overlord, northern Victoria Land, Antarctica: A window into high pressure storage and differentiation of mantle-derived basalts. *Lithos*, *268*, 225–239. https://doi.org/10.1016/j.lithos.2016.10.027

Pintér, Z., Patkó, L., Djoukam, J. F. T., Kovács, I., Tchouankoue, J. P., Falus, G., et al. (2015). Characterization of the sub-continental lithospheric mantle beneath the Cameroon volcanic line inferred from alkaline basalt hosted peridotite xenoliths from Barombi Mbo and Nyos Lakes. *Journal of African Earth Sciences*, *111*, 170–193. https://doi.org/10.1016/j.jafrearsci.2015.07.006

Powell, W., Zhang, M., O'Reilly, S. Y., & Tiepolo, M. (2004b). Mantle amphibole trace-element and isotopic signatures trace multiple metasomatic episodes in lithospheric mantle, western Victoria, Australia. *Lithos*, *75*(1–2), 141–171. https://doi.org/10.1016/j.lithos.2003.12.017

Prigent, C., Agard, P., Guillot, S., Godard, M., & Dubacq, B. (2018a). Mantle wedge (de) formation during subduction infancy: Evidence from the base of the semail ophiolitic mantle. *Journal of Petrology*, *59*(11), 2061–2092. https://doi.org/10.1093/petrology/egy090

Prigent, C., Guillot, S., Agard, P., Lemarchand, D., Soret, M., & Ulrich, M. (2018b). Transfer of subduction fluids into the deforming mantle wedge during nascent subduction: Evidence from trace elements and boron isotopes (Semail ophiolite, Oman). *Earth and Planetary Science Letters*, *484*, 213–228. https://doi.org/10.1016/j.epsl.2017.12.008

Raffone, N., Chazot, G., Pin, C., Vannucci, R., & Zanetti, A. (2009b). Metasomatism in the lithospheric mantle beneath Middle Atlas (Morocco) and the origin of Fe-and Mg-rich wehrlites. *Journal of Petrology*, *50*(2), 197–249. https://doi.org/10.1093/petrology/egn069

Rehfeldt, T., Foley, S. F., Jacob, D. E., Carlson, R. W., & Lowry, D. (2008). Contrasting types of metasomatism in dunite, wehrlite and websterite xenoliths from Kimberley, South Africa. *Geochimica et Cosmochimica Acta*, *72*(23), 5722–5756. https://doi.org/10.1016/j.gca.2008.08.020

Rivalenti, G., Mazzucchelli, M., Laurora, A., Ciuffi, S. I., Zanetti, A., Vannucci, R., & Cingolani, C. A. (2004). The backarc mantle lithosphere in Patagonia, South America. *Journal of South American Earth Sciences*, *17*(2), 121–152. https://doi.org/10.1016/j.jsames.2004.05.009

Rodriguez-Vargas, A., Koester, E., Mallmann, G., Conceição, R., Kawashita, K., & Weber, M. (2005). Mantle diversity beneath the Colombian Andes, northern volcanic zone: Constraints from Sr and Nd isotopes. *Lithos*, *82*(3–4), 471–484. https://doi.org/10.1016/j.lithos.2004.09.027

Rosatelli, G., Wall, F., & Stoppa, F. (2007b). Calcio-carbonatite melts and metasomatism in the mantle beneath Mt. Vulture (Southern Italy). *Lithos*, *99*(3–4), 229–248. https://doi.org/10.1016/j.lithos.2007.05.011

Sang, L., Vanpeteghem, C. B., Sinogeikin, S. V., & Bass, J. D. (2011). The elastic properties of diopside, $CaMgSi_2O_6$. *American Mineralogist*, *96*(1), 224–227. https://doi.org/10.2138/am.2011.3674

Saxena, A., & Langston, C. A. (2022). Detecting lithospheric discontinuities beneath the Mississippi Embayment using S-wave receiver functions. *Geophysical Journal International*, *228*(2), 744–754. https://doi.org/10.1093/gji/ggab367

Sinogeikin, S. V., & Bass, J. D. (2002). Elasticity of majorite and a majorite-pyrope solid solution to high pressure: Implications for the transition zone. *Geophysical Research Letters*, *29*(2), 4-1–4-4. https://doi.org/10.1029/2001gl013937

Smith, D., Riter, J. A., & Mertzman, S. A. (1999b). Water–rock interactions, orthopyroxene growth, and Si-enrichment in the mantle: Evidence in xenoliths from the Colorado Plateau, southwestern United States. *Earth and Planetary Science Letters*, *165*(1), 45–54. https://doi.org/10.1016/s0012-821x(98)00251-9

Spengler, D., & Alifirova, T. A. (2019). Formation of Siberian cratonic mantle websterites from high-Mg magmas. *Lithos*, *326*, 384–396. https://doi.org/10.1016/j.lithos.2018.12.020

Stosch, H.-G., & Lugmair, G. (1986). Trace element and Sr and Nd isotope geochemistry of peridotite xenoliths from the Eifel (West Germany) and their bearing on the evolution of the subcontinental lithosphere. *Earth and Planetary Science Letters*, *80*(3–4), 281–298. https://doi.org/10.1016/0012-821x(86)90111-1

Stosch, H.-G., & Seck, H. (1980). Geochemistry and mineralogy of two spinel peridotite suites from Dreiser Weiher, West Germany. *Geochimica et Cosmochimica Acta*, *44*(3), 457–470. https://doi.org/10.1016/0016-7037(80)90044-7

Sun, J., Liu, C.-Z., Kostrovisky, S. I., Wu, F.-Y., Yang, J.-H., Chu, Z.-Y., et al. (2017). Composition of the lithospheric mantle in the northern part of Siberian craton: Constraints from peridotites in the Obnazhennaya kimberlite. *Lithos*, *294*, 383–396. https://doi.org/10.1016/j.lithos.2017.10.010

Suzuki, I., & Anderson, O. L. (1983). Elasticity and thermal expansion of a natural garnet up to 1, 000K. *Journal of Physics of the Earth*, *31*(2), 125–138. https://doi.org/10.4294/jpe1952.31.125

Szabó, C., & Taylor, L. A. (1994b). Mantle petrology and geochemistry beneath the Nógrád-Gömör volcanic field, Carpathian-Pannonian region. *International Geology Review*, *36*(4), 328–358. https://doi.org/10.1080/00206819409465465

Turner, M., Turner, S., Blatter, D., Maury, R., Perfit, M., & Yogodzinski, G. (2017). Water contents of clinopyroxenes from sub-arc mantle peridotites. *Island Arc*, *26*(5), e12210. https://doi.org/10.1111/iar.12210

Wang, Q., Bagdassarov, N., Xia, Q.-K., & Zhu, B. (2014). Water contents and electrical conductivity of peridotite xenoliths from the North China Craton: Implications for water distribution in the upper mantle. *Lithos*, *189*, 105–126. https://doi.org/10.1016/j.lithos.2013.08.005

Wu, F.-Y., Walker, R. J., Yang, Y.-H., Yuan, H.-L., & Yang, J.-H. (2006). The chemical-temporal evolution of lithospheric mantle underlying the North China Craton. *Geochimica et Cosmochimica Acta*, *70*(19), 5013–5034. https://doi.org/10.1016/j.gca.2006.07.014

Xu, R., Liu, Y., Tong, X., Hu, Z., Zong, K., & Gao, S. (2013). In-situ trace elements and Li and Sr isotopes in peridotite xenoliths from Kuandian, North China Craton: Insights into Pacific slab subductionrelated mantle modification. *Chemical Geology*, *354*, 107–123. https://doi.org/10.1016/j.chemgeo.2013.06.022

Xu, W.-L., Gao, S., Yang, D.-B., Pei, F.-P., & Wang, Q.-H. (2009). Geochemistry of eclogite xenoliths in Mesozoic adakitic rocks from Xuzhou-Suzhou area in central China and their tectonic implications. *Lithos*, *107*(3–4), 269–280. https://doi.org/10.1016/j.lithos.2008.11.004

Xu, W., Hergt, J. M., Gao, S., Pei, F., Wang, W., & Yang, D. (2008). Interaction of adakitic melt-peridotite: Implications for the high-Mg# signature of Mesozoic adakitic rocks in the eastern North China Craton. *Earth and Planetary Science Letters*, *265*(1–2), 123–137. https://doi.org/10.1016/j.epsl.2007.09.041

Xu, X., O'Reilly, S. Y., Griffin, W., & Zhou, X. (2003b). Enrichment of upper mantle peridotite: Petrological, trace element and isotopic evidence in xenoliths from SE China. *Chemical Geology*, *198*(34), 163–188. https://doi.org/10.1016/s0009-2541(03)00004-4

Yang, W., Teng, F.-Z., & Zhang, H.-F. (2009). Chondritic magnesium isotopic composition of the terrestrial mantle: A case study of peridotite xenoliths from the North China Craton. *Earth and Planetary Science Letters*, *288*(3–4), 475–482. https://doi.org/10.1016/j.epsl.2009.10.009

Yu, H., Zhang, H.-F., & Santosh, M. (2017). Mylonitized peridotites of Songshugou in the Qinling orogen, central China: A fragment of fossil oceanic lithosphere mantle. *Gondwana Research*, *52*, 1–17. https://doi.org/10.1016/j.gr.2017.08.007

Zhang, J. S., & Bass, J. D. (2016). Sound velocities of olivine at high pressures and temperatures and the composition of Earth's upper mantle. *Geophysical Research Letters*, *43*(18), 9611–9618. https://doi.org/10.1002/2016gl069949

Zhang, Y.-L., Liu, C.-Z., Ge, W.-C., Wu, F.-Y., & Chu, Z.-Y. (2011). Ancient sub-continental lithospheric mantle (SCLM) beneath the eastern part of the Central Asian Orogenic Belt (CAOB): Implications for crust–mantle decoupling. *Lithos*, *126*(3–4), 233–247. https://doi.org/10.1016/j.lithos.2011.07.022

Zhao, X.-M., Zhang, H.-F., Zhu, X.-K., Zhu, B., & Cao, H.-H. (2015). Effects of melt percolation on iron isotopic variation in peridotites from Yangyuan, North China Craton. *Chemical Geology*, *401*, 96–110. https://doi.org/10.1016/j.chemgeo.2015.02.031

Zhao, X. M., Cao, H. H., Mi, X., Evans, N. J., Qi, Y. H., Huang, F., & Zhang, H. F. (2017). Combined iron and magnesium isotope geochemistry of pyroxenite xenoliths from Hannuoba, North China Craton: Implications for mantle metasomatism. *Contributions to Mineralogy and Petrology*, *172*(6), 1–26. https://doi.org/10.1007/s00410-017-1356-y

Zheng, J., Griffin, W. L., O'Reilly, S. Y., Yang, J., Li, T., Zhang, M., et al. (2006). Mineral chemistry of peridotites from Paleozoic, Mesozoic and Cenozoic lithosphere: Constraints on mantle evolution beneath eastern China. *Journal of Petrology*, *47*(11), 2233–2256. https://doi.org/10.1093/petrology/egl042